492 J. Med. Chem. 2010, 53, 492–498
DOI: 10.1021/jm9014795

Journal of Medicinal Chemistry Article

DNA Loop Sequence as the Determinant for Chiral Supramolecular Compound G-Quadruplex Selectivity

Haijia Yu,[†] Chuanqi Zhao,[†] Yong Chen,[‡] Manliang Fu,[†] Jinsong Ren,[†] and Xiaogang Qu*,[†]

[†]*Division of Biological Inorganic Chemistry, State Key Laboratory of Rare Earth Resource Utilization, Graduate School of the Chinese Academy of Sciences, Changchun Institute of Applied Chemistry, Chinese Academy of Sciences, Changchun, Jilin 130022, China, and* [‡]*College of Life Science, Jilin University, Changchun, Jilin 130012, China*

Received October 7, 2009

It is important to develop G-quadruplex binding agents that can discriminate between different quadruplexes. Recently we reported the first example that a chiral supramolecular complex can selectively stabilize human telomeric G-quadruplex among different G-quadruplex and duplex DNA, and the two enantiomers show different inhibition effect on telomerase activity. Here, we report that DNA loop sequence can be determinant for this chiral complex G-quadruplex selectivity. Adenine in the diagonal loop plays an important role in G-quadruplex hybrid structural transition, thus, it strongly influences the chiral complex induced DNA structural transition. The complex's preference for human telomeric DNA and its chiral selectivity prompted us to investigate whether the two enantiomers, M and P, can show different effects on cancer cells. The P enantiomer's chiral selectivity has been demonstrated in cancer cells by telomere shortening, β-galactosidase activity, and up-regulation of cyclin-dependent kinase inhibitors p16 and p21.

Introduction

Chiral molecular recognition of DNA is important for rational drug design and for developing structural probes of DNA conformation.[1−3] Human telomeric G-quadruplex is polymorphic and has been a promising drug target for cancer chemotherapy.[4−6] Chiral recognition of G-quadruplexes can provide a novel strategy for a generation of G-quadruplex selective chiral binders. Recently, we reported[7] the first example that a chiral supramolecular complex can distinguish different G-quadruplexes and selectively stabilize human telomeric G-quadruplex with chiral selectivity and show different activity against cancer cells. The chiral compound used, $[Ni_2L_3]^{4+}$, has a bimetallo triple helicate structure. Each enantiomer (M or P) has a hydrophobic surface and a compatible size with G-quartet, and the positive charged triple helical structure has the potential to interact with the loops and grooves of G-quadruplex.[7] Our results indicate that the P enantiomer can stabilize G-quadruplex DNA and convert G-quadruplex in sodium from antiparallel to hybrid structure, while the M enantiomer can not.[7] These chiral nonplanar ligands are different from conventional G-quadruplex binding agents because most G-quadruplex binding agents are composed of a planar and aromatic core,[6−10] which is designed for targeting the common G-tetrad in G-quadruplex DNA and therefore not capable of distinguishing different G-quadruplexes. Because the G-quadruplex sequence motifs are widespread in the human genome[8,9] and particularly enriched in gene promotors that can modulate transcription,[10,11] it is important to develop ligands that can distinguish different G-quadruplexes, specifically target human telomeric G-quadruplex, and understand their interaction mechanism. Here we are reporting that the DNA loop sequence can be determinant for chiral ligand G-quadruplex selectivity and the compound's chiral selectivity has been demonstrated in cancer cells by telomere shortening, β-galactosidase activity, and up-regulation of cyclin-dependent kinase (CDK[a]) inhibitors p16 and p21. The results will provide new insights into the mechanism of chiral ligands G-quadruplex selectivity and their effects on cancer cells.

Results and Discussion

All DNA we used in this study (Figure 1) can form a quadruplex structure in sodium or in potassium, which is confirmed by ultraviolet (UV) melting, circular dichroism (CD), and gel electrophoresis (Figure S1−S3). The chiral metallo-supramolecular compound we used,[7] $[Ni_2L_3]^{4+}$ (Figure 1C), is a tetracationic triple helical cylinder structure with four positive charges, a hydrophobic surface, and a size (length ~18 Å, diameter ~8 Å) compatible with G-quartet (length ~14 Å, width ~11 Å).[12] It is well-known that G-quadruplex DNA is polymorphic. Both G-quadruplex topology and stability are influenced by several factors, such as cations, base modification, loop length, and composition.[13−18] These factors would further affect molecular recognition of G-quadruplexes.[19−22] We find that the variation of the DNA loop can change chiral ligand G-quadruplex selectivity.

The P enantiomer can distinguish different telomeric G-quadruplex DNA.[7] For P enantiomer binding to human telomeric G-quadruplex DNA,[7] its binding affinity is about 2.6×10^7 M^{-1}, and the stoichiometry is 1:1. A notable difference between human and tetrahymena or oxytricha telomeric G-quadruplex is the adenine base in their loop.[7,23−26] We substituted thymines for the three adenines

*To whom correspondence should be addressed. Tel.: 86-431-8526-2656. Fax: 86-431-85262656. E-mail: xqu@ciac.jl.cn.

[a]Abbreviations: UV, Ultraviolet; CD, Circular Dichroism; CDK, cyclin-dependent kinase; hTel, human telomeric G-quadruplex; RTQ-PCR, quantitative real time PCR; TRF, terminal restriction fragment analysis; SA-β-gal, senescence-associated β-galactosidase.

 Published on Web 11/13/2009

A

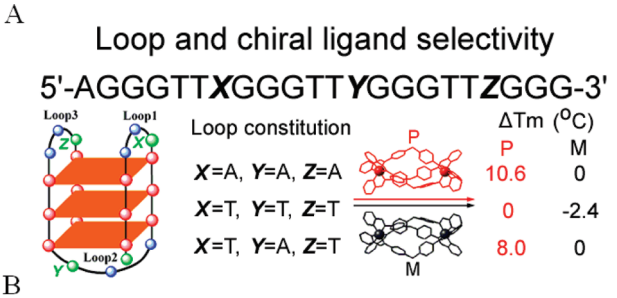

B

5'-AGGG-Loop1-GGG-Loop2-GGG-Loop3-GGG-3'

oligo name	Loop1	Loop 2	Loop3
hTel22	TTA	TTA	TTA
hTel-1	TTT	TTT	TTT
hTel-2	ATT	ATT	ATT
hTel-3	TAT	TAT	TAT
hTel-4	TTT	TTA	TTT
hTel-5	TTA	TTT	TTA
hTel-6	TTA	TTTT	TTA

C

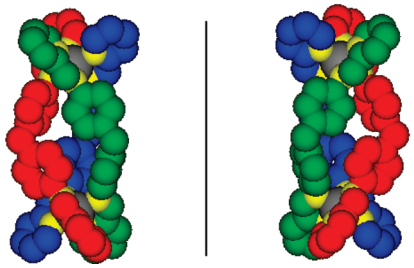

Figure 1. (A) Schematic representation of loop effect on chiral compound G-quadruplex selectivity; (B) DNA sequences used in this work. (C) Structure of the M-enantiomer (left) and P-enantiomer (right) of $[Ni2L3]^{4+}$ cation. Nickel, gray; nitrogen, yellow; carbon, red, green, and blue, which represent three ligand strands respectively.

Table 1. Stabilization Effect of M (1 μM) and P Enantiomer (1 μM) on Different DNA[a]

	Na^+			K^+		
DNA sequence	T_m (°C)	ΔT_m,[b] M (°C)	ΔT_m, P (°C)	T_m (°C)	ΔT_m, M (°C)	ΔT_m, P (°C)
hTel22	59.6	0	10.6	69.6	11.7	19.8
hTel-1	61.2	−2.4	0	79.7	0.8	1.9
hTel-2	47.7	0	0	69.1	4.6	7.7
hTel-3	55.3	0	0	75.6	3.2	4.1
hTel-4	56.2	0	8.0	74.6	4.1	9.5
hTel-5	64.8	−0.5	2.9	76.1	3	5.8
hTel-6	69.8	−0.3	−0.8	69.9	2.5	3.3

[a] In 10 mM Tris, 100 mM NaCl (or 10 mM KCl), pH 7.2 buffer. [DNA] = 1 μM/strand. T_m was determined by DNA UV melting studies. [b] $\Delta T_m = T_{m(\text{Compound-DNA})} - T_m$.

in loops (hTel-1, Figure 1) to examine the role of adenine. Neither the M nor the P enantiomer can stabilize hTel-1 in sodium (Table 1) at 1:1 binding ratio.[7] For wild-type human telomeric G-quadruplex (hTel22), a delayed new band appeared in P enantiomer binding.[7] However, for sample hTel-1, no new band was observed for either M or P enantiomer binding (Figure 2, lanes 1−3). The replacements of loop TTA with TTT diminish the chiral selectivity, indicating that the TTA loop is important for chiral ligand recognition and consistent with previous results of M or P enantiomer binding to tetrahymena or oxytricha telomeric DNA.[7]

A

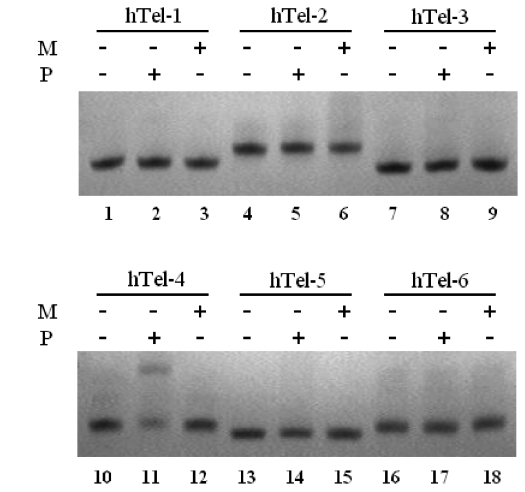

B

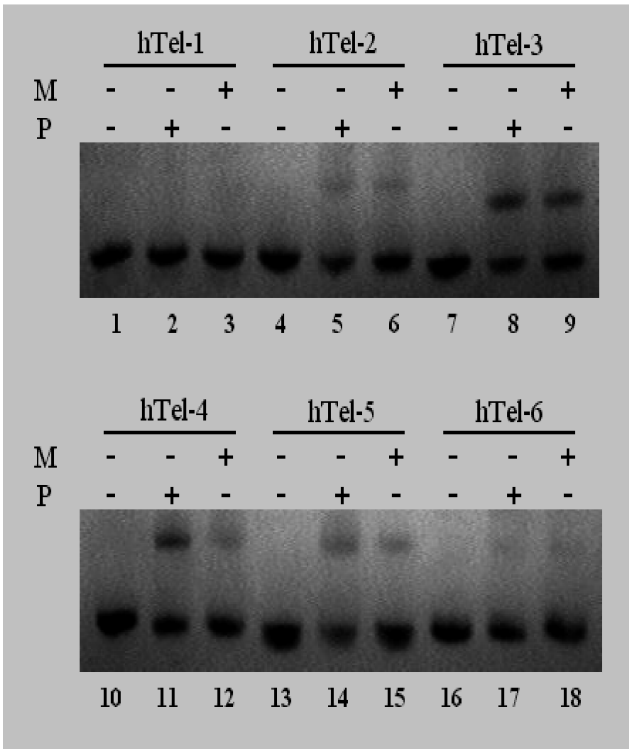

Figure 2. (A) Native gel electrophoretic analysis (20% PAGE) of DNA in the presence of P or M enantiomer. The gels were run in 1× TB buffer with 10 mM NaCl; (B) Native gel electrophoretic analysis (20% PAGE) of DNA in the presence of the P or M enantiomer. The gels were run in 1× TB buffer with 10 mM KCl.

Next, we further study the role of adenine in TTA loop by changing loop sequence. The interaction of the M or P enantiomer with hTel-2 or hTel-3 was similar as with hTel-1 (Figure 1B and Table 1). Neither the M nor the P enantiomer can stabilize DNA in sodium and no delayed new band was observed in gel (Figure 2, lanes 4−9). CD spectra of hTel-1, hTel-2, and hTel-3 all show a positive band at 295 nm and a negative band at 265 nm indicating that they form antiparallel structure in sodium (Figures S4−S6). M and P enantiomer binding only altered DNA CD intensity without hybrid conversion showing that nonspecific electrostatic interaction

happened, similar to previous reports.[7,27] Therefore, TTA loops are essential for the chiral selectivity of the G-quadruplex.

Previous studies have shown that the P enantiomer preferentially binds to the end of the G-quartet by external stacking and contact with the two lateral loops[7] (loops 1 and 3). However, unexpectedly, the TTA sequence in the diagonal loop (loop 2, Figure 1A) is more important for the chiral selectivity. When changing loop 1 and loop 3 to TTT and keeping loop 2 TTA unchanged (hTel-4, Figure 1B), the P enantiomer can still stabilize hTel-4 (the increase of melting temperature, ΔT_m = 8.0 °C at 1:1 ratio of [complex]/[DNA], Table 1), but M cannot. Both M and P enantiomers were stable under UV melting experimental conditions.[7] These results indicate that the P enantiomer remains chiral selectivity. When just changing loop 2 to TTT (hTel-5, Figure 1B), the P enantiomer can slightly stabilize hTel-5 (ΔT_m = 2.9 °C at 1:1 binding ratio). As for hTel-6, with an additional thymine in loop 2 (TTTT), the P enantiomer does not stabilize hTel-6 at all. This was further confirmed by gel electrophoresis (Figure 2). A delayed new band was only observed when the P enantiomer binds to hTel-4 (Figure 2, lane 11). Our next CD studies indicate that loop 2 is responsible for hybrid transition induced by P enantiomer binding.

CD spectrum of hTel-4 (Figure S7A) has a positive band at 292 nm and a small negative band near 270 nm in Na^+, which may indicate that hTel-4 predominantly form an antiparallel structure in Na^+.[7] Upon P enantiomer binding, the positive band shifted from 292 to 289 nm, which shows a hybrid-like feature formed in K^+ (Figure S7B), and the negative band turned positive simultaneously and shifted from 270 to 265 nm. The same trend has been observed when the P enantiomer binds to the wild-type human telomeric G-quadruplex.[7] This indicates that the P enantiomer prefers hybrid structure and can convert hTel-4 from antiparallel to hybrid structure in Na^+, just like P enantiomer binding to hTel22.[7] For the M enantiomer, it can not induce hTel22 or hTel-4 to have structural transition. In the case of hTel-5 and hTel-6 DNA, both of them adopt a typical antiparallel structure (Figures S8 and S9). M and P enantiomer binding to hTel-5 just decreased the negative band intensity at 265 nm without obvious band shift, although the decrease upon P enantiomer binding was stronger than M enantiomer. As for hTel-6, both M and P enantiomers show almost no influence on the DNA secondary structure. It is in accordance with UV melting and gel electrophoresis results that the P enantiomer shows chiral selectivity just for hTel-4 and hTel22.

We also studied chiral ligand G-quadruplex selectivity in K^+. CD spectra show that all DNA we used can form a hybrid structure in K^+ (Figure S3). Both M and P enantiomers can stabilize all the quadruplexes, including hTel-1, however, the stabilization effect of the P enantiomer is much stronger than M (Table 1), showing that the P enantiomer has stronger chiral selectivity[7] even in K^+. DNA CD spectra in K^+ buffer change little in the presence of M or P enantiomers, which may suggest that both enantiomers favor the hybrid form, however, in Na^+ buffer, the energetic cost of hybrid conversion favors P enantiomer binding. A delayed new band was also observed in K^+ for all DNA except hTel-1 (Figure 2B), although gel electrophoresis is not as sensitive as DNA melting data, which can show slightly different ligand binding affinity to this series of DNA sequences. As shown in Table 1, from hTel-1 to hTel-6, the effect of the P enantiomer on melting temperature is not identical. Besides hTel-22, the P enantiomer shows the strongest effect on hTel-4 and the least effect on hTel-1, consistent with the results in Na^+. This further supports that TTA in loop 2 is essential for P enantiomer chiral selectivity.

Table 2. Thermodynamic Parameters of DNA Alone and upon Binding of $[Ni_2L_3]^{4+}$-M (M) and $[Ni_2L_3]^{4+}$-P (P) [a]

DNA	ΔH (kJ/mol)	ΔS (J/mol·K)	$\Delta G_{37\,°C}$ (kJ/mol)
hTel22	−172.4 ± 1.1	−518.8 ± 3.1	−11.5 ± 2.0
hTel22+M	−146.1 ± 0.8	−438.1 ± 2.3	−10.2 ± 1.5
hTel22+P	−165.1 ± 1.3	−484.6 ± 3.8	−14.8 ± 1.5
hTel-1	−175.6 ± 0.3	−525.6 ± 1.0	−12.6 ± 0.6
hTel-1+M	−146.0 ± 0.9	−441.4 ± 2.8	−9.1 ± 1.8
hTel-1+P	−159.0 ± 0.8	−476.4 ± 2.3	−11.2 ± 1.5
hTel-4	−163.9 ± 1.0	−498.9 ± 3.1	−9.2 ± 2.0
hTel-4+M	−141.8 ± 0.7	−431.9 ± 2.2	−7.9 ± 1.4
hTel-4+P	−160.3 ± 1.3	−476.8 ± 3.8	−12.4 ± 1.5

[a] In 10 mM Tris, 100 mM NaCl, pH 7.2 buffer. For hTel22, $\Delta\Delta G_{37\,°C} = \Delta G_P - \Delta G_M$ = −4.6 kJ/mol; for hTel-4, $\Delta\Delta G_{37\,°C}$ = −4.5 kJ/mol; Thermodynamic parameters were calculated according to ref 5.

NMR studies[23] have shown that the base A13 in loop 2 of human telomeric G-quadruplex DNA in sodium is abnormal for its glycosidic torsion angle. 2-Ap fluorescence studies[28] also indicate that A13 is more stacked than the other two adenines in loops 1 and 3 both in Na^+ and in K^+. These results demonstrate that A13 in loop 2 is important for G-quadruplex topology. In combination with our CD studies, it can be seen that A13 in the diagonal loop is critical for hybrid structural transition. For wild-type (hTel22) and hTel-4, they have the same diagonal loop sequence TTA. This can be the reason why the P enantiomer can only induce hTel-4 and wild-type (hTel22) from antiparallel to hybrid structural transition and shows chiral selectivity (Table 1). At physiological temperature, 37 °C, the free energy difference estimated from DNA melting studies,[5] $\Delta\Delta G_{37°C} = \Delta G_{DNA\text{-}P} - \Delta G_{DNA\text{-}M}$, is about −4.6 kJ/mol (Table 2) for both wild-type (hTel22) and hTel-4, showing more favorable for P binding. Detailed structural studies are clearly needed to clarify the unique role of A13 for G-quadruplex topology and for structural transition.

Recently, a number of G-quadruplex forming regions have been identified in the gene promoters and many of them can be potential targets for therapeutic intervention.[10,11] This requires G-quadruplex binding agents to have the capability to discriminate different quadruplexes.[7,29] Our previous studies have shown that this complex can distinguish different telomeric G-quadruplexes.[7] Here we studied two other important G-quadruplexes that have been widely used in ligand binding, c-myc Pu27(5′-TGGGGAGGGTGGGGAGGG-TGGGGAAGG-3′) and c-kit (5′-AGGGAGGGCGCTGG-GAGGAGGG-3′).[10,11] C-myc Pu27 exists in the NHE element of the c-myc gene promoter[10] and forms a parallel G-quadruplex structure. Both M and P enantiomers can slightly increase c-myc quadruplex melting temperature (ΔT_m = 2∼3 °C, Table 3) and do not show chiral preference. This indicates that the P enantiomer has a more than 6-fold selectivity[7] (Table 3) for human telomeric G-quadruplex over the promoter c-myc, because P enantiomer can increase hTel22 T_m about 20 °C under the same conditions. For another proto-oncogene promotor c-kit,[11] both M and P enantiomers can significantly decrease c-kit quadruplex stability (ΔT_m = −9 °C, Table 3) and do not show chiral selectivity.

These encouraging results prompted us to investigate whether the two enantiomers, M and P, can show chiral

Table 3. Stabilization Temperature (ΔT_m) of Different G-Quadruplexes by P (1 μM) and M Enantiomer (1 μM) in 10 mM Tris Buffer Containing 10 mM KCl at pH 7.2[a]

	ΔT_m[b] (°C)		
chiral complex	hTel22	c-myc	c-kit
P enantiomer	19.8	2.7	−8.2
M enantiomer	11.7	2.4	−9.8

[a] The DNA concentration was 1 μM/strand. T_m was determined by DNA UV melting studies. [b] $\Delta T_m = T_{m(Compound\text{-}DNA)} - T_{m(DNA)}$.

selectivity in cancer cells. We have reported that the P enantiomer has a much stronger inhibition effect on telomerase activity than the M enantiomer.[7] Here the quantitative real time PCR(RTQ-PCR) results indicate that the P enantiomer can cause more rapidly telomere shortening in K562 cells than the M enantiomer (Figure 3A), showing chiral selectivity. The RTQ-PCR method has been widely used to detect telomere length[30−36] and can avoid overestimation of the telomere length, which can occur when using the terminal restriction fragment analysis (TRF) method.[37] Therefore, we used the RTQ-PCR method to avoid overestimation in this study. Based on the results of the short-term cell viability and the value of IC_{50} (Table S1), which was determined by MTT method, the long-term treatment concentrations of 1 μM P or M enantiomer used are far below the IC_{50} values and have no effect on short-term cell viability (Figure 3A). After treatment with the P enantiomer for 35 days, the telomere length of the K562 cell decreased 55% compared with the untreated group, whereas for the M enantiomer group, it decreased only 18%. The initial TRF length of K562 measured by Southern blotting was 7.3 kb;[38] despite the existence of a subtelomeric region in the TRF fragment, we could approximately assess that the telomere lost about 4 kb in the P enantiomer group and 1.3kb in the M enantiomer group. Ultimately, the telomere length decreased 68% or 5 kb at 55−60 days for P enantiomer treated groups and did not decrease any more. Thus, the telomere length may have decreased to the critical mean length necessary to maintain cell division in the K562 cell. The population doubling plateau occurred at 55−60 days[39] (Figure 3B). In the M enantiomer treated group, the cells still can proliferate after 60 days, but population doubling time was obviously increased (Figure 3B). Morphologic examination of the cells at the plateau phase indicates the increased proportion of flat and giant cells with phenotypic characteristics of senescence and overexpression of β-galactosidase activity[39] in the P enantiomer treated group is more obvious than in the M treated group (Figure 4). The positive staining for senescence-associated β-galactosidase (SA-β-gal) demonstrates that the P enantiomer can induce K562 cells senescence after continuous treatment. Further analysis indicates that the percentage of senescent cells is about 7, 25, and 50% for mock, M enantiomer, and P enantiomer treated groups, respectively. Besides, P enantiomer is more efficient to up-regulate expression[40,41] of CDK inhibitors p16 and p21 in K562 cells than M enantiomer (Figure 3C). Quantitative analysis was performed using Lab works 4.5 software (Ultraviolet Products, Upland, CA) and showed that the M enantiomer can up-regulate p16 and p21 expression about 5-fold, while the P enantiomer can increase p16 expression about 31-fold and p21 expression about 24-fold. CDK inhibitors p16 and p21 have been considered key effectors of cellular senescence.[42−44] Up-regulations of p16 and p21 suggest that these chiral complexes can induce cell-growth arrest and senescence mediated by overexpression of p16 and p21.

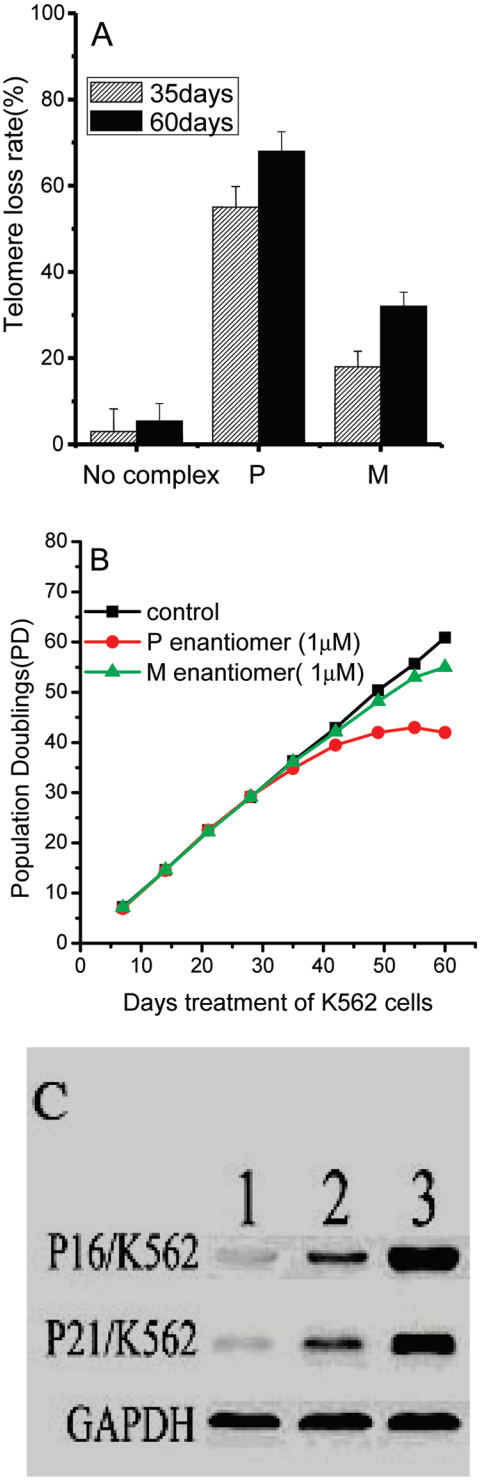

Figure 3. (A) Effects of M and P enantiomers on telomere length of K562 cells after treatment for 35 or 60 days. [M] or [P] concentration was 1 μM; (B) Senescence induced by M and P enantiomers on K562 cells. Cells were exposed to 1 μM M enantiomer (green data), 1 μM P enantiomer (red data), or no complexes as control (black data), respectively. The errors were within 10%. (C) Western blotting analysis of the p16 and p21 proteins after treatment with M and P enantiomers. After K562 cells were treated with one of the four complexes for 60 days, cells were lysed and separated on 12% SDS−PAGE. p16 and p21 protein levels were detected by Western blotting with antibodies against p16 and p21. Lane 1, control; lane 2, M enantiomer (1 μM); lane 3, P enantiomer (1 μM). Each experiment presented in A−C has been done three times. Experimental details were described in the Experimental Section.

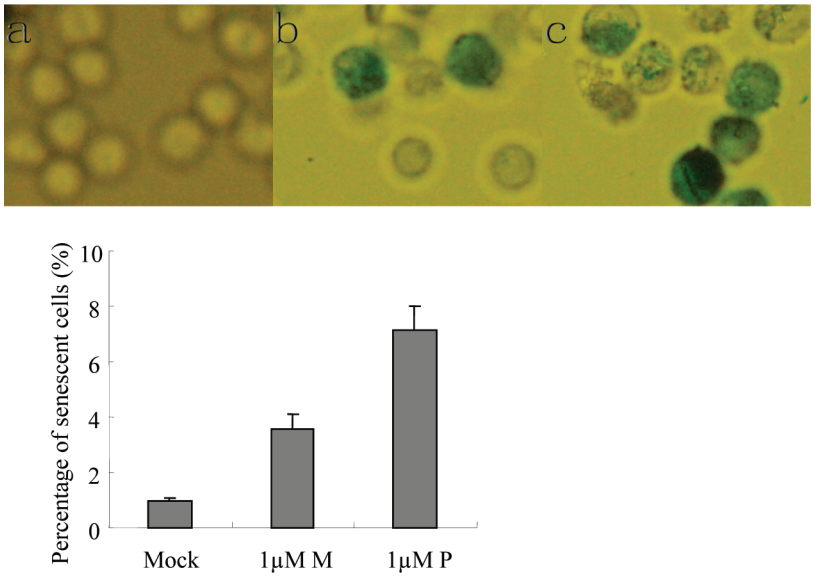

Figure 4. Expression of senescence-associated β-galactosidase (SA-β-gal) in K562 cells after continuous M and P enantiomer treatment. K562 cells were treated with (a) no complex; (b) 1 μM M enantiomer; and (c) 1 μM P enantiomer continuously for 60 days. Flat and giant cells with phenotypic characteristics of senescence and overexpression of β-galactosidase activity were detected in the P enantiomer treated group and partly in M treated groups. This assay was performed in triplicate. The senescent cells were counted under an inverted microscope in five random fields.

We are aware that cell senescence response can be induced by telomere erosion or by a number of stressful stimuli, for example, agents causing intracellular oxidative stress or persistent mitogenic stimulation. These stimuli induce an acute form of senescence, which occurs without the need for extensive cell proliferation.[45] Unlike these agents, the chiral complex did not induce cytotoxicity immediately after administration because complete inhibition of K562 cell proliferation requires continued cell division until the telomeres reach a critically short length. These observations indicate that K562 cell senescence is induced by disruption of telomere

Conclusion

Our studies demonstrate that the DNA loop sequence can be the determinant for chiral ligand G-quadruplex selectivity. Adenine in the diagonal loop plays an important role in G-quadruplex hybrid structural transition, thus it strongly influences chiral ligand induced DNA structural transition. Changing diagonal loop TTA to TTT can eliminate P enantiomer chiral selectivity. The complex human telomeric G-quadruplex selectivity prompts us to study and compare the effects of the two enantiomers on cancer cells. We have demonstrated the compound's chiral selectivity in cancer cells by telomerase inhibition, telomere shortening, β-galactosidase activity, and up-regulation of CDK inhibitors p16 and p21. Our work will provide new insights into understanding chiral ligand G-quadruplex selectivity and their different effects on cancer cells.

Experimental Section

5′-AGGGTTAGGGTTAGGGTTAGGG-3′ (human telomeric G-quadruplex) and its analogues with modifications in loops, c-myc Pu27 (5′-TGGGGAGGGTGGGGAGGGTGGGGAAGG-3′) and c-kit (5′-AGGGAGGGCGCTGGGAGGAGGG-3′), and other DNA oligomers were purchased from Sangon (Shanghai, China) and used without further purification. Concentrations of these oligomers were determined by measuring the absorbance at 260 nm after melting.[5−7] Extinction coefficients were estimated by the nearest-neighbor method by using mononucleotide and dinucleotide values.[5−7] All the experiments were carried out in 10 mM Tris buffer with 100 mM NaCl or 100 mM KCl, pH 7.2, unless stated otherwise.

The metallo-supramolecular cylinder $[Ni_2L_3]Cl_4$ was synthesized and purified as previously reported.[7] The enantiomerically pure $[Ni_2L_3]Cl_4$ was obtained by using a cellulose (~20 μm, Aldrich) column and eluting with 20 mM NaCl aqueous solution. The purity is more than 95%, which was determined by ESI-MS and elemental analysis.[7] UV−vis spectroscopy was used to determine the enantiomer concentration. The samples of purified M and P enantiomer were collected and freeze-dried for future use.[7]

Absorbance measurements and melting experiments were carried out on a Cary 300 UV/vis spectrophotometer equipped with a Peltier temperature control accessory.[5−7] All UV/vis spectra were measured in 1.0-cm-path-length cell with the same concentration of corresponding metal complex aqueous solution as the reference solution. Absorbance changes at 295 nm versus temperature were collected at a heating rate of 1 °C·min^{-1}. Thermodynamic parameters of DNA oligomers in the absence or presence of a chiral compound were estimated by using their melting profiles, according to a well-established method.[5] The enthalpy change, $\triangle H$, was determined from the temperature dependence of equilibrium association constant, where $\triangle H$ was the slope of ln K_a versus $1/T$ plot according to the equation $\ln(K_a) = -(\triangle H/RT) + \triangle S/R$, where $\triangle S$ was the entropy change that was obtained according to the y-axis intercept. The free energy change ($\triangle G$) at 37 °C was calculated from the standard Gibbs's equation, $\triangle G = \triangle H - T\triangle S$.

CD spectra were measured on a JASCO J-810 spectropolarimeter equipped with a temperature controlled water bath.[5−7] The optical chamber of CD spectrometer was deoxygenated with dry purified nitrogen (99.99%) for 45 min before use and kept the nitrogen atmosphere during experiments. Three scans were accumulated and automatically averaged. The various concentrations of M or P cylinder were scanned as a control and subtracted from the spectra of metal cylinder/DNA mixture to eliminate its influence on DNA CD signal between 340 and 220 nm.

Native gel electrophoresis[5−7] was carried out on acrylamide gel (20%) and run at 4 °C, 12.5 V/cm in 1× TB buffer containing 10 mM NaCl or 10 mM KCl, and was stained by stains-all.

Cell Line. The leukemia cell line K562[40,41] was cultured in Iscove's Modified Dulbecco's Medium (IMDM) and supplemented with 10% fetal bovine serum at 37 °C in a 5% CO_2 humidified incubator. The medium was exchanged once per two days.

Short-Term Cell Viability Assay by MTT. Cell viability was measured by the MTT method as we described before.[41,46] Briefly, K562 cells in the logarithmic growth-phase were collected, and 2×10^4 cells/well were dispensed within 96-well culture plates in 100 μL volumes. M and P enantiomers with different concentrations were added inside the 96-well plates. Three parallel wells were set for each of the treated or control groups. Culture plates were incubated for 72 h at 37 °C in a humidified atmosphere of 5% CO_2, and then 10 μL of MTT reagents (5 mg/mL) was added to each well. The cells were incubated for another 4 h at 37 °C, and then the liquid in the wells was evaporated. Solubilization solution (10% SDS in 0.01 M HCl; 100 μL) was added, and the absorbance (570 nm) was measured to estimate cell viability.

Long-Term Exposure Studies. Cells were grown in T25 tissue culture flasks at 2.0×10^5/flask. To avoid short-term apoptosis and other nonspecific effects on cells that could render the detection of telomeric events difficult, nonacute cytotoxic concentration (90% survival) were applied on K562 cells for long-term exposure every 3 days. The cells in control and drug-exposed flasks were collected and counted using a hematocytometer and flasks reseeded with 2.0×10^5 cells. Remaining cells were collected and used for measurements as described below. This weekly process, with twice-weekly complex addition, was continued until such time that there were fewer than 2.0×10^5 cells for reseeding.

Telomere Length Measurement by Quantitative Real-Time Polymerase Chain Reaction (PCR). Genomic DNA was extracted from each cell sample, and relative telomere length was measured using a real-time quantitative PCR method described by Cawthon,[30] with minor modifications. The technique measured the factor by which the sample differed from a reference DNA sample in its ratio of telomere repeat copy number to single copy gene copy number. This ratio was proportional to the average telomere length. A revised primer set[47] (Tel1 and Tel2) was used for telomere amplification and acidic ribosomal phosphoprotein P0 (RPLP0) gene primers (36B4) used as a single-copy gene reference. Each 20 μL PCR reaction included 10 μL 2× Syber Green PCR Master Mix (TaKaRa Biotech Ltd.), 20−100 ng genomic DNA, and primers at final concentrations: 200 nM for each telomere primer or 300 nM for each of the 36B4 primers. The amplification was performed in a ROCHE Light cycler system using the following conditions: 95 °C for 1 min, followed by 40 cycles of 95 °C for 15 s, 58 °C for 15 s, and 72 °C for 40 s for the 36B4 reaction, or 35 cycles of 95 °C for 15 s, 56 °C for 15 s, and 72 °C for 60 s for the telomere reaction. To determine the cycle threshold (C_t) value, two separate PCR runs were performed for each sample and primer pair. To serve as a reference for standard curve calculation, the genomic DNA extracted from untreated cell sample was serially diluted from 3.125 to 100 ng per well. The LightCycler software was used for the construction of the standard curve and calculation of the C_t values. The relative telomere/single copy gene ratio (T/S value) was calculated using the formula $T/S \approx 2^{\Delta\Delta C_t}$, where $\Delta\Delta C_t = \Delta C_{t(\text{sample})} - \Delta C_{t(\text{control})}$, and $\Delta C_t = C_{t(36B4)} - C_{t(\text{Tel})}$.

Senescence-Associated β-Galactosidase (SA-β-gal) Assay. The senescent status was verified by staining for SA-β-gal as described.[48] Cells treated with each of the four complexes were washed twice in PBS, fixed in 2% formaldehyde/0.2% glutaraldehyde for 5 min at room temperature, washed again in PBS, and incubated for 16 h with β-Gal stain solution containing 1 mg/mL 5-bromo-4-chloro-3-indolyl-β-D-galactoside, 40 mM citric acid/sodium phosphate, pH 6, 5 mM potassium ferrocynide, 5 mM potassium ferricyanide, 150 mM NaCl, and 2 mM $MgCl_2$. Cells were viewed with use of a light microscope and photographed at ×400 magnification.

Western Blotting.[40,41] After treatment, the cells were washed with PBS, and lysed in 100 mL of lysis buffer (10 mM Tris-HCl, pH 7.4, 5 mM $MgCl_2$, 1 mM EDTA, 25 mM NaF, fresh 100 mM Na_3VO_4, and l mM dithiothreitol). Cell lysates were centrifuged for 10 min at 14000 g. Concentrations of protein in the supernatant were determined by BCA protein assay. Equal amounts of protein (40 μg) were resolved on 15% SDS−PAGE and transferred electrophoretically to PVDF membrane. The membranes were blocked with blocking buffer (6% casein, 1% polyvinylpyrrolidone, 10 mM EDTA) in TBST (10 mM Tris-HCl, pH 7.4, 150 mM NaCl, 0.1% Tween-20), and then incubated with mouse monoclonal anti-$p21^{WAF1}$ and anti-$p16^{INK4a}$ (Thermo Fisher Scientific, Fremont, CA) for 2 h at room temperature, washed three times with TBST for 30 min, and then incubated with alkaline phosphatase conjugated secondary antibody (ZSGB-BIO Inc., Beijing, China) for 2 h at room temperature. After washing the secondary antibody, the bound antibody complex was incubated in BCIP/NBT reagents and then photographed.

Acknowledgment. The authors are grateful to Prof. Y. Zheng (Central Laboratory of the second Hospital, Jilin University) for his technical assistance. This project was supported by NSFC (20831003, 90813001, 20833006) and Funds from CAS.

Supporting Information Available: Supporting table and figures. This material is available free of charge via the Internet at http://pubs.acs.org.

References

(1) Xu, Y.; Zhang, Y. X.; Sugiyama, H.; Umano, T.; Osuga, H.; Tanaka, K. (P)-helicene displays chiral selection in binding to Z-DNA. *J. Am. Chem. Soc.* **2004**, *126*, 6566–6567.
(2) Qu, X.; Trent, J. O.; Fokt, I.; Priebe, W.; Chaires, J. B. Allosteric, chiral-selective drug binding to DNA. *Proc. Natl. Acad. Sci. U.S.A.* **2000**, *97*, 12032−12037 and cited references.
(3) Barton, J. K. Metals and DNA: molecular left-handed complements. *Science* **1986**, *233*, 727–734.
(4) Mergny, J. L.; Helene, C. G-quadruplex DNA: a target for drug design. *Nat. Med.* **1998**, *4*, 1366–1367.
(5) Li, X.; Peng, Y.; Ren, J.; Qu, X. Carboxyl-modified single-walled carbon nanotubes selectively induce human telomeric i-motif formation. *Proc. Natl. Acad. Sci. U.S.A.* **2006**, *103*, 19658−19663 and cited references.
(6) Ren, J.; Qu, X.; Trent, J. O.; Chaires, J. B. Tiny telomere DNA. *Nucleic Acids Res.* **2002**, *30*, 2307–2315.
(7) Yu, H.; Wang, X.; Fu, M.; Ren, J.; Qu, X. Chiral metallosupramolecular complexes selectively recognize human telomeric G-quadruplex DNA. *Nucleic Acids Res.* **2008**, *36*, 5695−5703 and cited references.
(8) Todd, A. K.; Johnston, M.; Neidle, S. Highly prevalent putative quadruplex sequence motifs in human DNA. *Nucleic Acids Res.* **2005**, *33*, 2901–2907.
(9) Verma, A.; Halder, K.; Halder, R.; Yadav, V. K.; Rawal, P.; Thakur, R. K.; Mohd, F.; Sharma, A.; Chowdhury, S. Genome-wide computational and expression analyses reveal G-quadruplex DNA motifs as conserved cis-regulatory elements in human and related species. *J. Med. Chem.* **2008**, *51*, 5641–5649.
(10) Siddiqui-Jain, A.; Grand, C. L.; Bearss, D. J.; Hurley, L. H. Direct evidence for a G-quadruplex in a promoter region and its targeting with a small molecule to repress c-MYC transcription. *Proc. Natl. Acad. Sci. U.S.A.* **2002**, *99*, 11593–11598.
(11) Phan, A. T.; Kuryavyi, V.; Burge, S.; Neidle, S.; Patel, D. J. Structure of an unprecedented G-quadruplex scaffold in the human c-kit promoter. *J. Am. Chem. Soc.* **2007**, *129*, 4386–4392.
(12) De Cian, A.; Delemos, E.; Mergny, J. L.; Teulade-Fichou, M. P.; Monchaud, D. Highly efficient G-quadruplex recognition by bisquinolinium compounds. *J. Am. Chem. Soc.* **2007**, *129*, 1856–1857.
(13) Gray, R. D.; Chaires, J. B. Kinetics and mechanism of K^+- and Na^+-induced folding of models of human telomeric DNA into G-quadruplex structures. *Nucleic Acids Res.* **2008**, *36*, 4191–4203.
(14) Mekmaysy, C. S.; Petraccone, L.; Garbett, N. C.; Ragazzon, P. A.; Gray, R.; Trent, J. O.; Chaires, J. B. Effect of O6-methylguanine on

the stability of G-quadruplex DNA. *J. Am. Chem. Soc.* **2008**, *130*, 6710–6711.
(15) Smargiasso, N.; Rosu, F.; Hsia, W.; Colson, P.; Baker, E. S.; Bowers, M. T.; De Pauw, E.; Gabelica, V. G-quadruplex DNA assemblies: Loop length, cation identity, and multimer formation. *J. Am. Chem. Soc.* **2008**, *130*, 10208–10216.
(16) Li, W.; Wu, P.; Ohmichi, T.; Sugimoto, N. Characterization and thermodynamic properties of quadruplex/duplex competition. *FEBS Lett.* **2002**, *526*, 77–81.
(17) Olsen, C. M.; Lee, H. T.; Marky, L. A. Unfolding thermodynamics of intramolecular G-quadruplexes: Base sequence contributions of the loops. *J. Phys. Chem. B* **2009**, *113*, 2587–2595.
(18) Guédin, A.; Alberti, P.; Mergny, J. L. Stability of intramolecular quadruplexes: Sequence effects in the central loop. *Nucleic Acids Res.* **2009**, *37*, 5559–5567.
(19) Seenisamy, J.; Bashyam, S.; Gokhale, V.; Vankayalapati, H.; Sun, D.; Siddiqui-Jain, A.; Streiner, N.; Shin-Ya, K.; White, E.; Wilson, W. D.; Hurley, L. H. Design and synthesis of an expanded porphyrin that has selectivity for the c-MYC G-quadruplex structure. *J. Am. Chem. Soc.* **2005**, *127*, 2944–2959.
(20) Arora, A.; Maiti, S. Effect of loop orientation on quadruplex-TMPyP4 interaction. *J. Phys. Chem. B* **2008**, *112*, 8151–8159.
(21) Miyoshi, D.; Karimata, H.; Wang, Z. M.; Koumoto, K.; Sugimoto, N. Artificial G-wire switch with 2,2′-bipyridine units responsive to divalent metal ions. *J. Am. Chem. Soc.* **2007**, *129*, 5919–5925.
(22) Antonacci, C.; Chaires, J. B.; Sheardy, R. D. Biophysical characterization of the human telomeric (TTAGGG)4 repeat in a potassium solution. *Biochemistry* **2007**, *46*, 4654–4660.
(23) Wang, Y.; Patel, D. J. Solution structure of the human telomeric repeat d[AG3(T2AG3)3] G-tetraplex. *Structure* **1993**, *1*, 263–282.
(24) Wang, Y.; Patel, D. J. Solution structure of the Tetrahymena telomeric repeat d(T2G4)4 G-tetraplex. *Structure* **1994**, *2*, 1141–1156.
(25) Wang, Y.; Patel, D. J. Solution structure of the Oxytricha telomeric repeat d[G4(T4G4)3] G-tetraplex. *J. Mol. Biol.* **1995**, *251*, 76–94.
(26) Dai, J.; Punchihewa, C.; Ambrus, A.; Chen, D.; Jones, R. A.; Yang, D. Structure of the intramolecular human telomeric G-quadruplex in potassium solution: A novel adenine triple formation. *Nucleic Acids Res.* **2007**, *35*, 2440–2450.
(27) Xu, H.; Zhang, H.; Qu, X. Interactions of the human telomeric DNA with terbium-amino acid complexes. *J. Inorg. Biochem.* **2006**, *100*, 1646–1652.
(28) Li, J.; Correia, J. J.; Wang, L.; Trent, J. O.; Chaires, J. B. Not so crystal clear: the structure of the human telomere G-quadruplex in solution differs from that present in a crystal. *Nucleic Acids Res.* **2005**, *33*, 4649–4659.
(29) Shirude, P. S.; Gillies, E. R.; Ladame, S.; Godde, F.; Shin-Ya, K.; Huc, I.; Balasubramanian, S. Macrocyclic and helical oligoamides as a new class of G-quadruplex ligands. *J. Am. Chem. Soc.* **2007**, *129*, 11890–11891.
(30) Cawthon, R. M. Telomere measurement by quantitative PCR. *Nucleic Acids Res.* **2002**, *30*, e47.
(31) Demerath, E. W.; Cameron, N.; Gillman, M. W.; Towne, B.; Siervogel, R. M. Telomeres and telomerase in the fetal origins of cardiovascular disease: A review. *Hum. Biol.* **2004**, *76*, 127–146.
(32) Epel, E. S.; Blackburn, E. H.; Lin, J.; Dhabhar, F. S.; Adler, N. E.; Morrow, J. D.; Cawthon, R. M. Accelerated telomere shortening in response to life stress. *Proc. Natl. Acad. Sci. U.S.A.* **2004**, *101*, 17312–17315.
(33) Guillot, P. V.; Gotherstrom, C.; Chan, J.; Kurata, H.; Fisk, N. M. Human first-trimester fetal MSC express pluripotency markers and grow faster and have longer telomeres than adult MSC. *Stem Cells* **2007**, *25*, 646–654.
(34) Harris, S. E.; Deary, I. J.; MacIntyre, A.; Lamb, K. J.; Radhakrishnan, K.; Starr, J. M.; Whalley, L. J.; Shiels, P. G. The association between telomere length, physical health, cognitive aging, and mortality in non-demented older people. *Neurosci. Lett.* **2006**, *406*, 260–264.
(35) Martin-Ruiz, C.; Saretzki, G.; Petrie, J.; Ladhoff, J.; Jeyapalan, J.; Wei, W.; Sedivy, J.; von Zglinicki, T. Stochastic variation in telomere shortening rate causes heterogeneity of human fibroblast replicative life span. *J. Biol. Chem.* **2004**, *279*, 17826–17833.
(36) Wolf, D.; Rumpold, H.; Koppelsttäer, C.; Gastl, G. A.; Steurer, M.; Mayer, G.; Gunsilius, E.; Tilg, H.; Wolf, A. M. Telomere length of in vivo expanded CD4(+)CD25(+) regulatory T-cells is preserved in cancer patients. *Cancer Immunol. Immunother.* **2006**, *55*, 1198–1208.
(37) O'Callaghan, N. J.; Dhillon, V. S.; Thomas, P.; Fenech, M. A quantitative real-time PCR method for absolute telomere length. *Biotechniques* **2008**, *44*, 807–809.
(38) Asai, A.; Oshima, Y.; Yamamoto, Y.; Uochi, T. A.; Kusaka, H.; Akinaga, S.; Yamashita, Y.; Pongracz, K.; Pruzan, R.; Wunder, E.; Piatyszek, M.; Li, S.; Chin, A. C.; Harley, C. B.; Gryaznov, S. A novel telomerase template antagonist (GRN163) as a potential anticancer agent. *Cancer Res.* **2003**, *63*, 3931–3939.
(39) Riou, J. F.; Guittat, L.; Mailliet, P.; Laoui, A.; Renou, E.; Petitgenet, O.; Mégnin-Chanet, F.; Hélène, C.; Mergny, J. L. Cell senescence and telomere shortening induced by a new series of specific G-quadruplex DNA ligands. *Proc. Natl. Acad. Sci. U.S.A.* **2002**, *99*, 2672–2677.
(40) Wang, X.; Ren, J.; Qu, X. Targeted RNA interference of cyclin A2 mediated by functionalized single-walled carbon nanotubes induces proliferation arrest and apoptosis in chronic myelogenous leukemia K562 cells. *ChemMedChem* **2008**, *3*, 940–945.
(41) Wang, X.; Song, Y.; Ren, J.; Qu, X. Knocking-down cyclin A_2 by siRNA suppresses apoptosis and switches differentiation pathways in K562 cells upon administration with doxorubicin. *PLoS One* **2009**, *4*, e6665.
(42) Feldser, D. M.; Greider, C. W. Short telomeres limit tumor progression in vivo by inducing senescence. *Cancer Cell* **2007**, *11*, 461–469.
(43) Cosme-Blanco, W.; Shen, M.-F.; Lazar, A. J. F.; Pathak, S.; Lozano, G.; Multani, A. S.; Chang, S. Telomere dysfunction suppresses spontaneous tumorigenesis in vivo by initiating p53-dependent cellular senescence. *EMBO Rep.* **2007**, *8*, 497–503.
(44) Gunaratnam, M.; Shen, M. F.; Lazar, A. J.; Pathak, S.; Lozano, G.; Multani, A. S.; Chang, S. Mechanism of acridine-based telomerase inhibition and telomere shortening. *Biochem. Pharmacol.* **2007**, *74*, 679–689.
(45) Serrano, M.; Blasco, M. A. Putting the stress on senescence. *Curr. Opin. Cell Biol.* **2001**, *13*, 748–753.
(46) Shangguan, G.; Xing, F.; Qu, X.; Mao, J.; Zhao, D.; Zhao, X.; Ren, J. DNA binding specificity and cytotoxicity of novel antitumor agent Ge132 derivatives. *Bioorg. Med. Chem. Lett.* **2005**, *15*, 2962–2965.
(47) Gil, M. E.; Coetzer, T. L. Real-time quantitative PCR of telomere length. *Mol. Biotechnol.* **2004**, *27*, 169–172.
(48) Dimri, G. P.; Lee, X.; Basile, G.; Acosta, M.; Scott, G.; Roskelley, C.; Medrano, E. E.; Linskens, M.; Rubelj, I.; Pereira-Smith, O.; Peacocke, M.; Campisi, J. A biomarker that identifies senescent human cells in culture and in aging skin in vivo. *Proc. Natl. Acad. Sci. U.S.A.* **1995**, *92*, 9363–9367.